PRediction Of Geospace Radiation Environment and Solar wind parameterS

Work Package 6
Forecast of the radiation belt environment

Deliverable 6.3
Results of the VNC model and two methods of model coupling

Alastair Williamson, Simon Walker,
Yuri Shprits, and Angelica Tibocha

December 3, 2018

This project has received funding from the *European Union's Horizon 2020 research and innovation programme* under grant agreement No 637302.

Document Change Record

Issue	Date	Author	Details
1.0	2018-07-16	A. Williamson	Initial draft
1.1	2018-07-23	S. Walker	Updates
1.2	2018-07-24	A. Williamson	
2	2018-09-24	S. Walker	Updates following RM4

Contents

Summary

Work package 6 aims to improve the forecasting of electron fluxes in the radiation belt environment. With this in mind, Task T6.3 aims to improve the results of simulations of the electron fluxes by providing a more realistic estimate of the electron outer boundary flux.

Two methods for the coupling of the NARMAX electron flux forecasts at Geostationary Equatorial Orbit (GEO) to the VERB outer boundary at $L^* = 7\ R_e$ are investigated. The first assumes that GEO lies at a fixed radial distance of $L^* = 6.2 R_e$. This value was chosen as it represents an average value of L^* of GEO. The second method uses a varying value of L^*. Since the terrestrial magnetic field moves in response to geomagnetic activity, the value of L^* at a specific location will vary. In this coupling method, the value of L^* is calculated using the IRBEM-lib library of source codes. The Tsyganenko 89c magnetic field model, which requires the Kp geomagnetic index as input, is used for the field line tracing. It is shown that this addition can result in large changes in the initialisation of the parameters at the VERB outer boundary.

1 Introduction

Work Package 6 deals with the forecast of the radiation belt environment. Task T6.1 developed a set of models (SNB^{3}GEO) for the forecast of electron fluxes at various energies at Geostationary Equatorial Orbit that were reported in deliverable D6.1. These flux models have proven to be highly successful and their performance has been shown to be slightly better than other models, notably the Relativistic Electron Forecast Model (REFM) at NOAA (*Balikhin et al.*, 2016). Unfortunately these models are restricted to geostationary orbit due to the fact that they are data driven and there is only sufficient data coverage at GEO. Thus these models cannot say anything about the electron fluxes in regions away from this specific orbit. In order to get a wider picture of the spatial electron distribution throughout the radiation belt region we require either a far greater

spatial/temporal coverage of measurements or a method to extrapolate the results at GEO throughout the rest of the inner magnetosphere. This latter option is possible through the use of numerical simulation codes.

Within PROGRESS we use the VERB (Versatile Electron Radiation Belt) (*Subbotin and Shprits*, 2009) numerical model to estimate the energetic (MeV) electron distributions within this region. VERB solves the Fokker-Planck equation in 3D, incorporating the processes of radial diffusion and the diffusion of particles in both energy and pitchangle due to wave-particle interactions. However, deliverable D6.3 makes use of the 1D output from VERB in a similar vein to e.g. *Shprits* (2009); *Shprits et al.* (2009). The main inputs to VERB are the *Kp* index and an estimate of the electron boundary flux at the location L^*=7R_e.

The *Kp* index is used to define the level of geomagnetic activity on a quasi-logarithmic scale between 0-9 and is readily available from GFZ Potsdam. Following on from deliverable D6.1 (NARMAX modelling at a GEO) it is possible to derive the flux at L^*=7R_e, as required by VERB, as shown in Appendix A.

In this report we look into the coupling between VERB and NARMAX. As mentioned above, the model electron flux estimates from SNB^3 are available at GEO only. This orbit lies at a radial distance of L=6.6R_e and thus the model fluxes are measured/forecasted at this location. Since the terrestrial magnetic field not rotationally symmetric (being compressed on the dayside and elongated on the nightside in addition to the offset, tilted dipole axis) this distance will vary when expressed in L^* coordinates. The radial distance measured in L^* is also dependant upon geomagnetic activity. This report investigates two methods for the conversion of electron fluxes measured/forecast at L=6.6 R_e to the VERB outer boundary at L^*=7 R_e. In the first method we assume that the L^* position of geostationary orbit is independent of geomagnetic activity and is always situated at a radial distance of L^*_{GEO} = 6.2 R_e. In the second method of coupling we try to calculate the actual average value for L^*_{GEO} based on the Tsyganeko T89c model of the

geomagnetic field (*Tsyganenko*, 1989) which calculates the terrestrial magnetic field based on geomagnetic activity level as defined by the *Kp* index. The second coupling method should produce a more realistic value for L^*_{GEO} based on the current level of geomagnetic activity.

2 Methodology

The principle that the L^* radial position of a satellite at GEO changes is based upon the fact that the solar wind flow modifies the shape of the terrestrial field, compressing it on the day side and elongating it in to a tail on the night side. In addition, changes within the solar wind itself, such as increases in the particle density, pressure, and/or velocity, will result in further day side compression, distorting the magnetic field and giving rise to what is generally termed geomagnetic activity.

The radial distance of a satellite is often expressed as in terms of its L-shell (*McIlwain*, 1961), determined by tracing the magnetic field line at the measurement location to determine the radial distance (in R_e) at which it crosses the magnetic equator. The simple L-shell parameter has been superseded by a similar measurement, L^*, whose calculation is based on the third adiabatic invariant (*Roederer*, 1970) and signifies the radial distance of the field line in the equatorial plane if the magnetic field was adiabatically relaxed to a dipolar configuration.

The determination of the point at which the field line crosses the magnetic equator requires a realistic model for the terrestrial field. Examples of such models range from IGRF, a high order model of the inner magnetospheric dipole (see e.g. *Thébault et al.*, 2015), the Olson-Pfitzer quiet time model *Olson and Pfitzer* (1974) that describes the undisturbed geomagnetic field configuration to the highly sophisticated T04 *Tsyganenko* (2014), characterised by the state of the solar wind. In this report, the Tsyganenko 89c (*Tsyganenko*, 1989) model is used for field line tracing. This model uses the *Kp* index to characterise the shape of the terrestrial field based on the level of geomagnetic activ-

ity. The conversion from the measurement location to L^* is carried out using MATLAB routines from the IRBEM-lib library of source codes (*Bourdarie and OBrien*, 2009) (formerly known as ONERA-DESP-LIB) that is freely available. The electron boundary flux is estimated using NARMAX models (detailed in Appendix A) and is then propagated from the L^* position of geostationary orbit, estimated at 6.2 R_e for the initial parts of this work, to the VERB outer boundary at L^*=7 R_e.

3 Variation of L^* with time and Kp

As mentioned above, the default coupling between the electron flux models and VERB assumes that GEO lies at a fixed location of ${L^*}_{GEO}$ = 6.2 R_e regardless of time of day, time of year, or geomagnetic activity level. In this section we look at the variation of the location of GEO in L^* as functions of time and geomagnetic activity.

Figure 1 shows the variation in L^* of the location of GEO. The black, red, green, and blue traces are based on different times of the year, namely around the spring equinox, summer solstice, autumn equinox and winter solstice respectively. All traces exhibit a similar shape, varying between 5.8 R_e around midday and between 6.6–6.7 R_e at midnight. The average value of L^* on each of the dates varies between 6.24 and 6.26 R_e. The magenta line marks L^* = 6.2 R_e, the value used in the first method for coupling. The average distances for periods of Kp=1 and 2 are 6.1 R_e and 6.0 R_e respectively. Thus, for relatively low values of Kp, this assumption holds quite well.

However, as values of the Kp index increase to 3 and higher this assumption is no-longer true. Figure 2 shows the ${L^*}_{GEO}$ variation for Kp values of 0 (black), 3 (red), 5 (green), 7 (blue), and 9 (cyan) on 2015-03-21. Once again, the magenta line represents ${L^*}_{GEO}$ = 6.2 R_e. It is clearly seen that the location of GEO moves to lower L^* as Kp increases. The average values for ${L^*}_{GEO}$ are around 5.9, 5.3, and 4.8 for Kp values of 3, 5, and 7 respectively. Thus, changes in Kp can have a significant effect upon the average value of ${L^*}_{GEO}$.

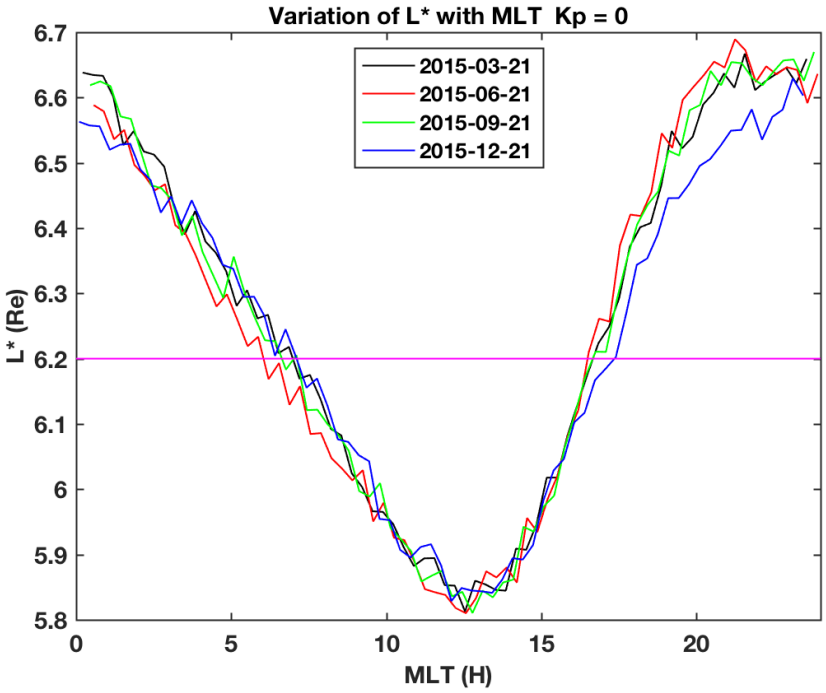

Figure 1: The variation of the L^* radial distance of GEO as a function of MLT for the the equinox and solstice dates in 2015 for a value of Kp=0.

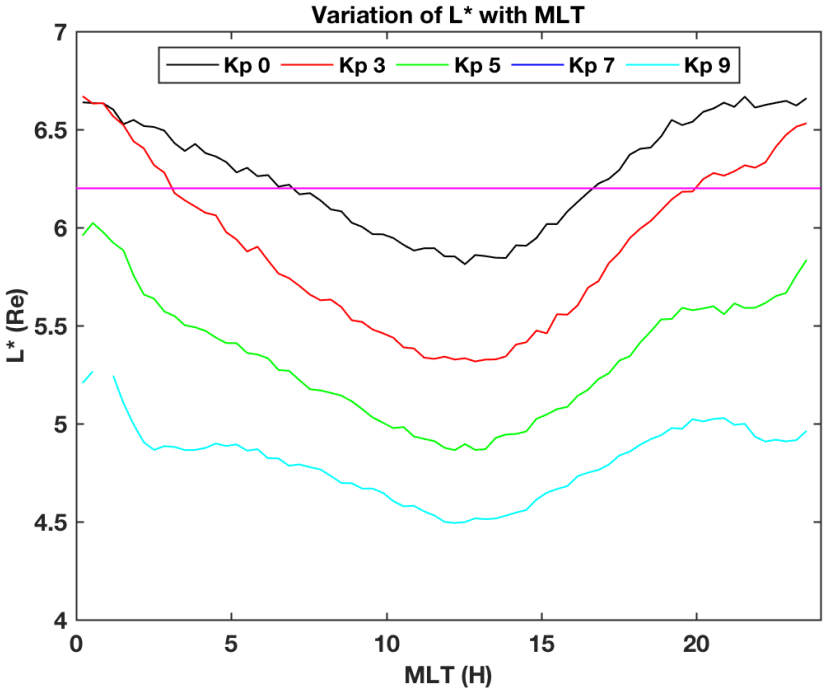

Figure 2: The variation of the L^*_{GEO} radial distance of as a function of MLT for the values of Kp = 0, 3, 5, 7, and 9 on 2015-03-21.

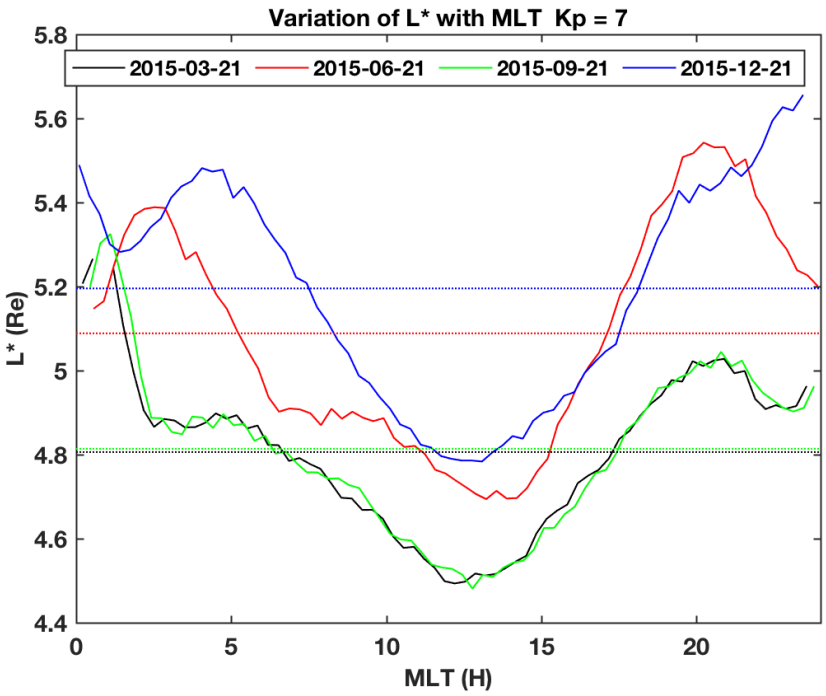

Figure 3: Variation of the L^*_{GEO} at different times of the year, with a high value of $Kp = 7$

It is noticeable from Figure 1 that the location of GEO in L^* does not show large changes related to the time of the year. This result does not hold for high values of Kp. Figure 3 shows the variation of L^*_{GEO} as a function of MLT for times around the spring (black) and vernal (green) equinoxes and the summer (red) and winter (blue) solstices. A high value for geomagnetic activity, $Kp = 7$, has been used. The dotted lines represent the averages of L^* for each date. It is clearly seen that the values of L^* around the equinoxes are very similar, in the range $4.5 < L^* < 5.3$, with an average of the order of 4.8 R_e. The solstice values, however, are quite different in profile. Around the summer solstice the location of GEO varies in the range 4.7–5.4 R_e averaging a value of around 5.1 R_e. The winter solstice date shows a variation in the range 4.8–5.6 R_e averaging around 5.2 R_e. Whilst all traces show the appearance of a peak or shoulder around 20MLT, the location of observed in the morning sector varies from 1 h MLT at the equinoxes to 2.5 h MLT in summer, and 5 h MLT in winter.

4 Changes in flux levels

Figures 1, 2, and 3 show that the location of GEO when measured in terms of L^* can vary quite considerably depending upon the level of geomagnetic activity as well as the time of year. We now investigate the change this has on the electron flux levels as they are mapped to the VERB outer boundary. The main assumption behind the mapping process is that the particle Phase Space Density (PSD) does not vary between GEO and the VERB outer boundary at $L^* = 7\ R_e$. From the GEO flux forecasts, the flux of 0.892 MeV energy electrons is computed (see Section A). Assuming conservation of the first adiabatic invariant

$$\begin{aligned} p_{GEO} &= \sqrt{\frac{E^2}{c^2} + 2m} \\ PSD_{GEO} &= \frac{f_{GEO}}{p_{GEO}^2} \\ \mu &= \frac{p_{GEO}^2 \sin^2(\alpha)}{2m_0 B} \end{aligned}$$

Assuming conservation of PSD

$$\begin{aligned} PSD_B &= PSD_{GEO} \\ p_B &= \sqrt{\frac{2\mu m_0 B}{\sin^2(\alpha)}} \\ f_B &= PSD_B p_B^2 \end{aligned}$$

where p, E, m, f, and α are the particle momentum, energy, mass, flux, and pitchangle respectively, at either Geostationary Orbit ($_{GEO}$) or the VERB outer boundary ($_B$), and B the local magnetic field.

From the previous section, the value of L^* for GEO can vary in the range $5 < L^* < 7$ for moderate values of Kp. The flux levels resulting from the interpolation of the NARMAX

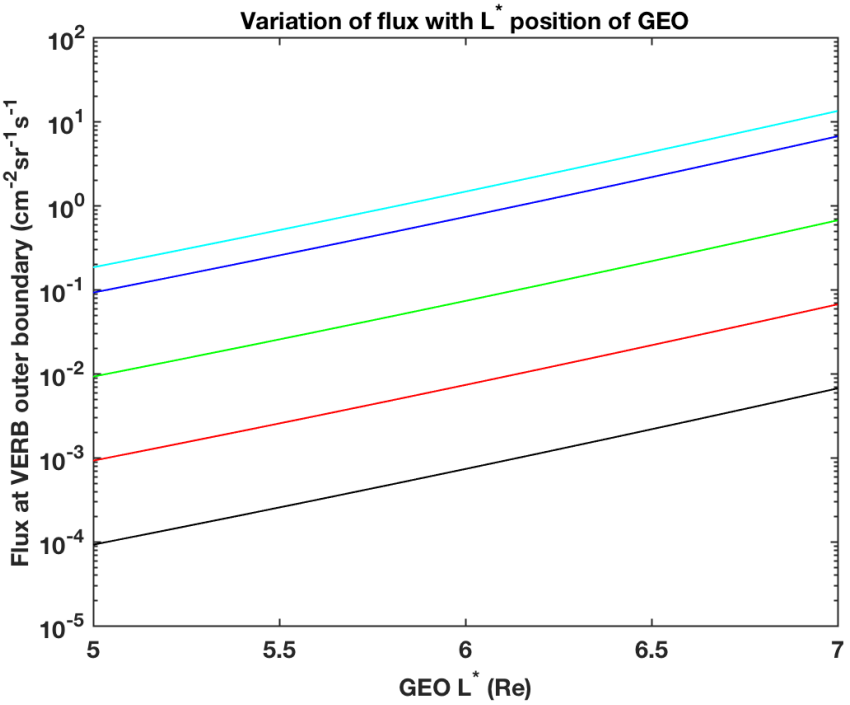

Figure 4: VERB output boundary electron flux as a function of L^*. The initial fluxes at GEO are 0.1 (black), 1 (red), 10 (green), 100 (blue), and 200 (cyan) $\mathrm{cm}^{-2}\mathrm{sr}^{-1}\mathrm{s}^{-1}$

flux model output can vary in the range $0.1 < f_{GEO} < 200$ $\mathrm{cm}^{-2}\mathrm{sr}^{-1}\mathrm{s}^{-1}$. Figure 4 shows the VERB output boundary electron flux as a function of L^* for GEO electron fluxes of 0.1 (black), 1 (red), 10 (green), 100 (blue), and 200 (cyan) $\mathrm{cm}^{-2}\mathrm{sr}^{-1}\mathrm{s}^{-1}$.

From Figure 4 it can be seen that the VERB outer boundary electron fluxes can vary by a factor of ≈ 16 as the value of L^*_{GEO} varies from 5 to 7. These changes can have a significant effect on the output electron energy spectra resulting from the VERB simulation. Figure 5 shows the results from four VERB runs that use constant values of Kp and boundary fluxes. These runs include radial, energy, pitchangle, and mixed term diffusion processes. The values used for Kp and the boundary flux are as follows: panel (a) Kp=0, bf=0.1, panel (b) Kp=0, bf=1.0, panel (c) Kp=7, bf=0.1, panel (d) Kp=7, bf=1.0. These panes show that the effect of changing Kp from zero to 7 is to move the location of the peak of the radiation belt inwards from L^* 6 at Kp=0 to $L^*\approx$ 3.5 under strongly geomagnetic conditions associated with Kp=7.

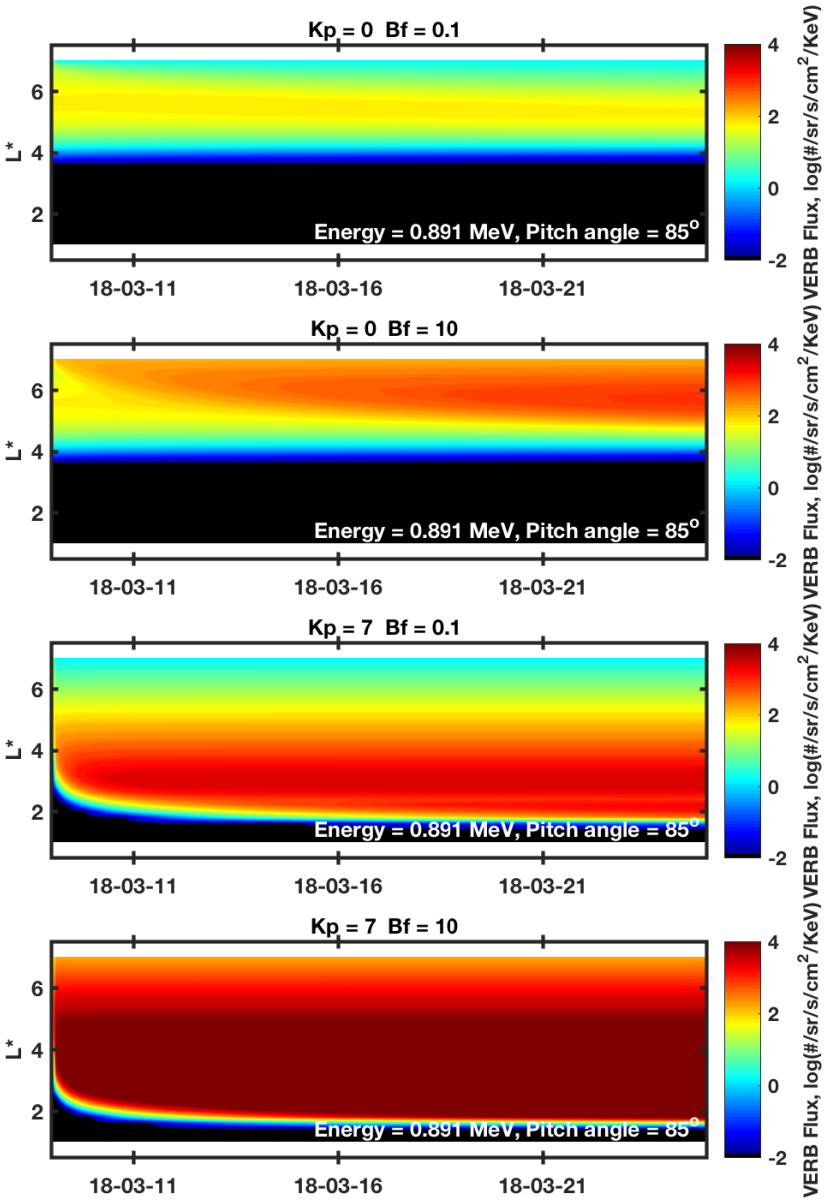

Figure 5: Example output from VERB using constant input values for Kp and boundary flux. The values used for Kp and the boundary flux are as follows: (a) Kp=0, bf=0.1, (b) Kp=0, bf=1.0, (c) Kp=7, bf=0.1, (d) Kp=7, bf=1.0.

5 Example event

In the previous sections the effects of modifying the L^*_{GEO} have been investigated. It was shown that as the level of geomagnetic activity increases the assumption that on average GEO lies at L^*_{GEO} =6.2$R_e$becomes invalid. Thus, in order to improve the electron spectra output from VERB it is necessary to modify L^* based on the current value of Kp in the estimation of the electron flux at the outer boundary position used by VERB. In this section we compare the results from two VERB simulations using a fixed and Kp driven values for the electron outer boundary flux with measurements from the Van Allen Probes A MagEIS instrument. The time period studied is 2015-03-08 to 2015-03-21. This period is notable for a geomagnetic storm that occurred on 2015-03-17.

Panel (a) of Figure 6 shows the variation in the Kp index measured in the period 2015-03-08 to 2015-03-21. At the beginning of this period, Kp is low, typically in the range $0 < Kp < 3$, indicating geomagnetically quiet conditions. However, on 2015-03-17 its value suddenly increases to Kp=7^+, evidence for intense geomagnetic activity initiated by a CME that erupted from the surface of the Sun two days before. When this CME struck the terrestrial magnetosphere it would have compressed the dayside such that the magnetopause moved inwards, encountering the radiation belts and resulting in the sudden loss of particles from this region. This change in the shape of the terrestrial field would lead to a change in the average L^* position of GEO. Panel (b) of Figure 6 shows how the average value of L^*_{GEO} varies during this time period. Until 2015-03-17 the average value of L^* varies over the narrow range 6.0 $<L^*<$ 6.3. During this period the initial coupling model that assumed GEO to be at a distance of L^*∼6.2 R_e would be expected to yield reasonable results. However, as the storm struck the L^*value of GEO changed dramatically, reducing to below 5 R_e before recovering to around L^*∼5.5 R_e by 2015-03-18, a day later. This change in the L^* radial location of GEO would result in changes to the electron flux at the L^*=7 R_e outer boundary that is required as an input to VERB. This change in the fluxes is shown in panel (c) of Figure 6. In this panel

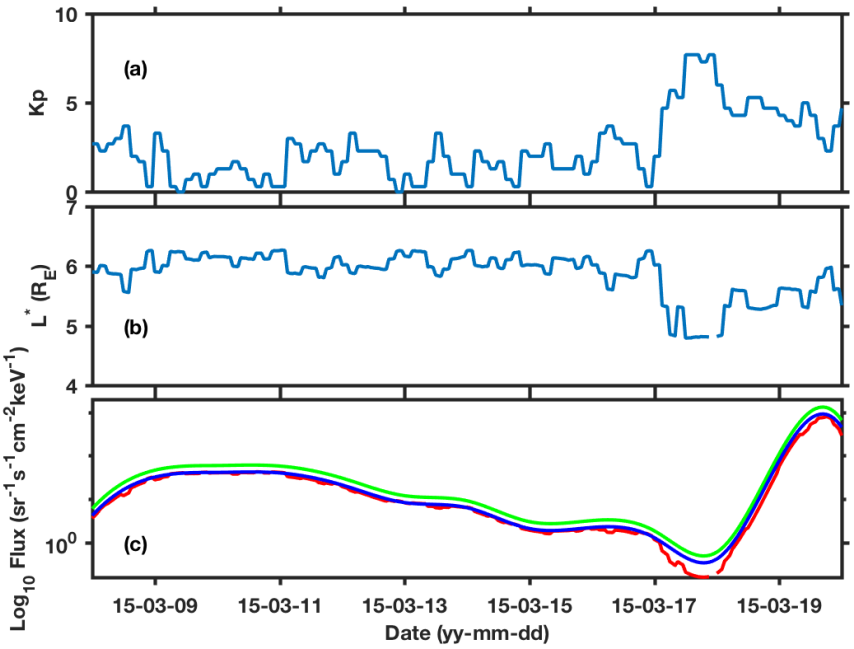

Figure 6: Variation of VERB input parameters during March 2015. Panel (a) shows Kp index, (b) the the Kp dependent average L^* for GEO, and (c) the measured/forecast flux at GEO (green), the VERB electron boundary flux calculated assuming constant L^* (blue) and variable L^* (red).

the green line represents the fluxes measured at GEO, calculated using the results of the SNB^{3}GEO models for the fluxes of >800keV and >2MeV electrons. This value is then propagated out to the VERB outer boundary under the assumption that the PSD remains constant. The results of this propagation are indicated by the blue line which uses the assumption of L^*_{GEO}=6.2 while the red curve is based the value of L^*_{GEO} changing with Kp. The blue and red curves are very similar in the period leading up to the geomagnetic storm, indicating that the assumption of L^*~6.2 R_e is a good estimate for low levels of geomagnetic activity. However, during the storm period the value of the boundary flux estimates vary by of the order 12% depending upon the coupling method used. It is seen that allowing L^*_{GEO} to vary with Kp actually reduces the value of the fluxes at the verb outer boundary.

Panels (a) and (b) of Figure 7 show the results of two VERB simulations using fixed

(upper) and variable (middle) values of L^*_{GEO} to determine the outer boundary electron fluxes. For both runs, it takes a day or so for the simulations to settle down to a realistic configuration. From 2015-03-09 until 2015-03-17 (i.e./ before the storm) both simulations show a similar radial spectrum of electrons with a peak in the distribution occurring just inside L^*=5 R_e. The similarity of these two sections of the simulations indicate that at low geomagnetic activity levels, the change in L^*_{GEO} is minimal and has little effect on the final simulations. On closer inspection it appears that the fluxes estimated using the fixed L^*_{GEO}=6.2 R_e are slightly higher than those using the Kp driven variable L^*_{GEO}. This reflects the fact that for Kp>2 the estimated boundary flux values are very slightly less, as seen in Figure 6. In comparison to actual measurements from the Van Allen Probes A MagEIS instrument both simulations show smaller and narrower peaks in the radial particle spectra which may indicate that some processes are operating that were not included within the VERB runs. At just after midday on 2015-03-17 the CME struck the terrestrial magnetosphere. At this time the value of Kp rises to around 7^+ (panel(a), Figure 6). From panel(c) of Figure 6 it is clear that this change in Kp causes a large change in the VERB outer boundary electron flux. At this point, the results of the two VERB simulations begin to differ significantly. Both show a sudden depletion of particles, first at higher L^* and then at lower. This processes is also observed in the actual observations but occurs a great deal faster. After this depletion period, the electron populations observed in the radiation belt region refill quickly, from lower L^* to higher with a considerable flux at L^*=3 R_e. Both simulations show about a day delay before this refilling process begins. This is most probably due to the fact that the forecast models used to calculate the initial electron flux at GEO are currently unable to replicate the rapid emptying and refilling of the radiation belts. The observation of large fluxes at lower L^* is not replicated particularly well in the results shown in Figure 7 panel (a) and is completely missing from the results shown in panel (b) that uses a variable L^*. This disappearance is currently being investigated.

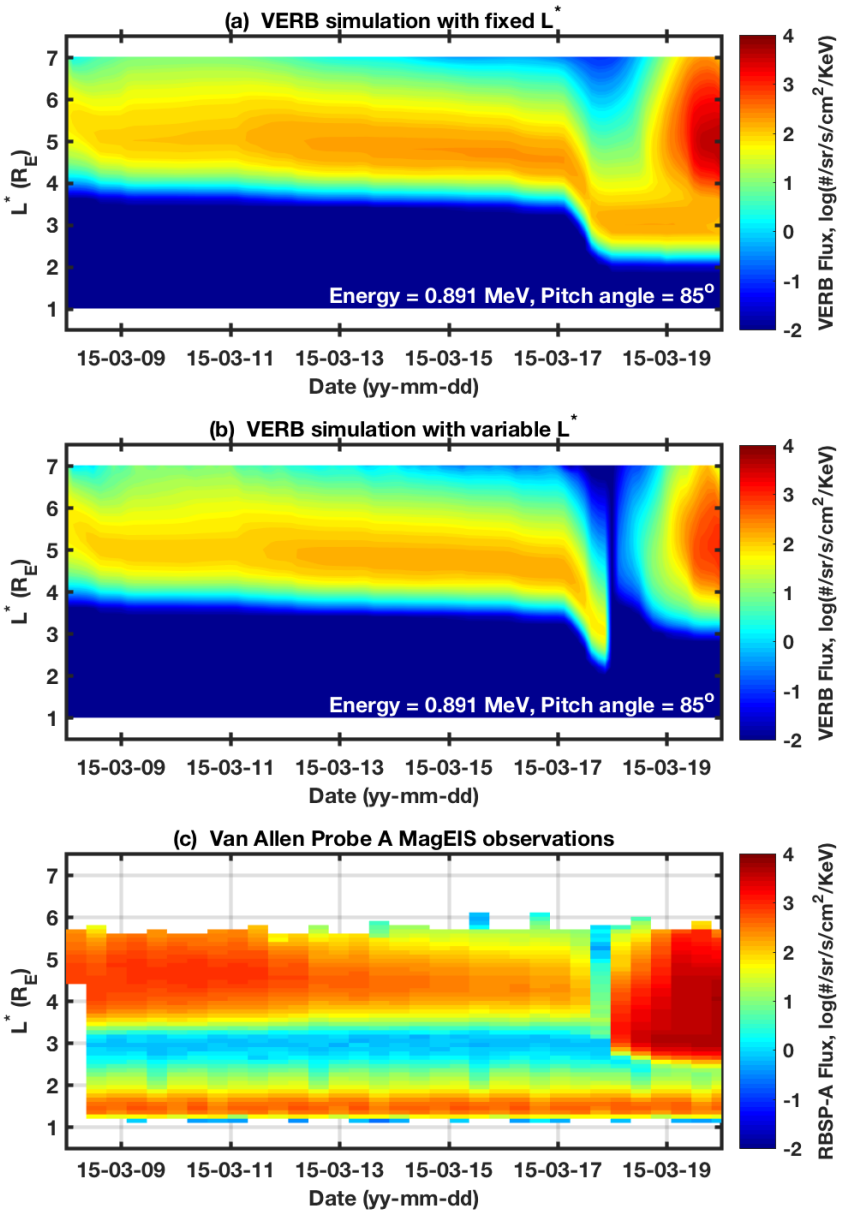

Figure 7: A comparison of Verb simulations and measurements from the Van Allen Probes A MagEIS instrument. The top panel shows the VERB output assuming a constant L^*_{GEO}=6.2 R_e. In the middle panel the value of L^*_{GEO} is allowed to vary based on the level of geomagnetic activity. The bottom panel shows MagEIS measurements.

6 Conclusions

In this report we have investigated the differences in two different coupling schemes used to join the NARMAX generated SNB^{3}GEO models for the fluxes of electrons at GEO with the VERB numerical code to estimate the fluxes of electrons throughout the radiation belt region. The first scheme assumes that the Geostationary Equatorial Orbit lies at a constant radial distance of L^*_{GEO} =6.2 R_e irrespective of geomagnetic activity level. The second scheme computes an average value for L^*_{GEO} based on the current level of geomagnetic activity.

It was shown that the assumption used in the first coupling methodology is only applicable for low values of Kp ($Kp \leq 2$). As Kp increases beyond Kp=2 the value of L^*_{GEO} begins to deviate from that used in the first coupling methodology. This change has a marked effect on the estimate of the electron flux levels that are used to seed the VERB simulation runs. The second method, that calculates an average value of L^*_{GEO} based on the current level of geomagnetic activity, provides a series of electron fluxes for the VERB outer electron boundary that is more realistic for higher levels of geomagnetic activity. These new boundary flux values enable VERB to model the variation in the radial electron spectrum more accurately than is possible using the fixed L^*_{GEO} coupling method.

References

Balikhin, M. A., J. V. Rodriguez, R. J. Boynton, S. N. Walker, H. Aryan, D. G. Sibeck, and S. A. Billings (2016), Comparative analysis of NOAA REFM and SNB^{3}GEO tools for the forecast of the fluxes of high-energy electrons at GEO, *Space Weather*, *14*, 22–31, doi:10.1002/2015SW001303.

Bourdarie, S., and T. P. OBrien (2009), International radiation belt en- vironment modelling library, cospar panel on radiation belt environment modelling (prbem), *Tech. rep.*, ONERA.

McIlwain, C. E. (1961), Coordinates for mapping the distribution of magnetically trapped particles, *J. Geophys. Res.*, *66*(11), 3681–3691, doi:10.1029/JZ066i011p03681.

Olson, W. P., and K. A. Pfitzer (1974), A quantitative model of the magnetospheric magnetic field, *J. Geophys. Res.*, *79*(25), 3739–3748, doi:10.1029/JA079i025p03739.

Roederer, J. G. (1970), *Dynamics of geomagnetically trapped radiation*, Springer-Verlag.

Shprits, Y. Y. (2009), Potential waves for pitch-angle scattering of near-equatorially mirroring energetic electrons due to the violation of the second adiabatic invariant, *Geophys. Res. Lett.*, *36*, L12106, doi:10.1029/2009GL038322.

Shprits, Y. Y., D. Subbotin, and B. Ni (2009), Evolution of electron fluxes in the outer radiation belt computed with the verb code, *J. Geophys. Res. (Space Physics)*, *114*(A13), A11209, doi:10.1029/2008JA013784.

Subbotin, D. A., and Y. Y. Shprits (2009), Three-dimensional modeling of the radiation belts using the versatile electron radiation belt (VERB) code, *Space Weather*, *7*, S10001, doi:10.1029/2008SW000452.

Thébault, E., C. C. Finlay, C. D. Beggan, P. Alken, J. Aubert, O. Barrois, F. Bertrand, T. Bondar, A. Boness, L. Brocco, E. Canet, A. Chambodut, A. Chulliat, P. Coïsson,

F. Civet, A. Du, A. Fournier, I. Fratter, N. Gillet, B. Hamilton, M. Hamoudi, G. Hulot, T. Jager, M. Korte, W. Kuang, X. Lalanne, B. Langlais, J.-M. Léger, V. Lesur, F. J. Lowes, S. Macmillan, M. Mandea, C. Manoj, S. Maus, N. Olsen, V. Petrov, V. Ridley, M. Rother, T. J. Sabaka, D. Saturnino, R. Schachtschneider, O. Sirol, A. Tangborn, A. Thomson, L. Tøffner-Clausen, P. Vigneron, I. Wardinski, and T. Zvereva (2015), International geomagnetic reference field: the 12th generation, *Earth, Planets, and Space*, *67*, 79, doi:10.1186/s40623-015-0228-9.

Tsyganenko, N. A. (1989), A magnetospheric magnetic field model with a warped tail current sheet, *Planet. Sp. Sci.*, *37*, 5–20, doi:10.1016/0032-0633(89)90066-4.

Tsyganenko, N. A. (2014), Data-based modeling of the geomagnetosphere with an imf-dependent magnetopause, *J. Geophys. Res. (Space Physics)*, *119*, 335–354, doi: 10.1002/2013JA019346.

A Calculation of electron flux estimates

NARMAX provides estimates of

- flux of electrons with energy greater than 800 keV
- flux of electrons with energy greater than 2 MeV

If we assume a Maxwellian distribution

$$J = A \times \exp(-B * E) \tag{1}$$

The constants A and B may be estimated from the results of the NARMAX SNB^{3}GEO models for the fluxes of electrons in the energy ranges $E >$800 keV and $E >$2MeV.

The NARMAX models provide the fluxes of particles greater than a lower energy limit, e.g.

$$\begin{aligned} J(E > E_1) &= \int_{E_1}^{\inf} J(E)\, dE \\ &= \int_{E_1}^{\inf} A \times \exp(-BE)\, dE \\ &= \left[-\frac{A}{B}\exp(-BE)\right]_{E_1}^{\inf} \\ &\approx \frac{A}{B}\exp(-BE) \end{aligned}$$

For energies $E_1 > 800$ keV

$$J_1(E > 800keV) = \frac{A\exp(-BE_1)}{B}$$

For energies $E_2 > 2000$ keV

$$J_2(E > 2000keV) = \frac{A\exp(-BE_2)}{B}$$

Taking logs

$$\begin{aligned} \log(J_1) &= \log\left(\frac{A}{B}\right) - BE_1 \\ \log(J_2) &= \log\left(\frac{A}{B}\right) - BE_2 \end{aligned}$$

and finding the difference in fluxes

$$\log(J_2) - \log(J_1) = -B(E_2 - E_1)$$

$$\frac{\log\left(\frac{J_2}{J_1}\right)}{(E_2 - E_1)} = -B$$

Substitute back into the expression for J_2 and rearrange to get A

$$A = \frac{BJ_2}{\exp(-BE_2)}.$$

Thus it is possible to estimate the flux at a specific energy as is required as an input to VERB.